Title: Removal of Pb and Cu ions from aqueous solution by Mn_3O_4-coated activated carbon

Author: Myoung-Eun Lee Jin Hee Park Jae Woo Chung Chae-Young Lee Seoktae Kang

PII: S1226-086X(14)00160-9
DOI: http://dx.doi.org/doi:10.1016/j.jiec.2014.03.006
Reference: JIEC 1952

To appear in:

Received date: 25-7-2013
Revised date: 12-12-2013
Accepted date: 5-3-2014

Please cite this article as: M.-E. Lee, J.H. Park, J.W. Chung, C.-Y. Lee, S. Kang, Removal of Pb and Cu ions from aqueous solution by Mn_3O_4-coated activated carbon, *Journal of Industrial and Engineering Chemistry* (2014), http://dx.doi.org/10.1016/j.jiec.2014.03.006

Removal of Pb and Cu ions from aqueous solution by Mn_3O_4-coated activated carbon

Myoung-Eun Lee[a], Jin Hee Park[b], Jae Woo Chung[a,*], Chae-Young Lee[c], Seoktae Kang[d]

[a]Department of Environmental Engineering, Gyeongnam National University of Science and Technology, Dongjin-ro 33, Jinju, Gyeongnam 660-758, Korea

[b]Center for Mined Land Rehabilitation, The University of Queensland, St. Lucia, QLD 4072, Australia

[c]Department of Civil Engineering, The University of Suwon, Wau, Bongdam, Hwaseong, Gyeonggi 445-758, Korea

[d]Department of Civil Engineering, Kyung Hee University, Giheung, Yongin, Gyeonggi 446-701, Korea

*Corresponding author tel: +82-55-751-3348; fax: +82-55-751-3848; e-mail: jwchung@gntech.ac.kr

ABSTRACT

Mn_3O_4-coated activated carbon (Mn_3O_4/AC) was prepared by supercritical technique and applied for the removal of Pb and Cu ions from aqueous solution. Kinetic and isotherm data of the adsorption by Mn_3O_4/AC were compared with those of activated carbon (AC) and pure Mn_3O_4. Adsorption of metals was adequately described by pseudo-second-order kinetics and Langmuir isotherm models. Maximum adsorption capacities of Pb and Cu ions determined by Langmuir model were enhanced 2.2 and 6.1 times for Pb and Cu ions by

Mn_3O_4 coating onto AC, which might be attributed to reduced resistance of intraparticle diffusion and enhanced surface electrostatic interaction and complexation by Mn_3O_4.

Keywords: Mn_3O_4-coated activated carbon; Adsorption; Lead; Copper; Kinetic; Isotherm

1. Introduction

Environmental pollution caused by heavy metals is deteriorating the environment and endangering human health. This has become a serious problem due to the toxic properties of heavy metals and their tendency to bio-accumulate in the food chain [1]. The presence of heavy metals in the aquatic environment is a major concern due to their extreme toxicity. Heavy metals from wastewater are commonly removed by chemical precipitation, ion-exchange, membrane separation, reverse osmosis, and activated carbon (AC) adsorption [2,3]. Adsorption has attracted much attention as an effective purification and separation technique for treating wastewater, and removing heavy metals from wastewater is an important application of adsorption processes using a suitable adsorbent [3,4]. Various adsorbents such as AC, iron oxides, filamentous fungal biomass, zeolite, and chitosan have been applied to remove heavy metals from wastewater. AC is generally recognized as an effective adsorbent due to its high porosity, large surface area, and high catalytic activity and is currently widely used to remove organic compounds [5]. However, AC has a relatively low adsorption capacity for inorganic pollutants compared to organic pollutants and requires longer time to remove contaminants [6,7].

Modifying AC with suitable additives has been investigated to enhance its adsorption efficacy [8]. Modified activated carbon studied includes palladium, silver, copper sulphide

and zinc oxide nanoparticle loaded activated carbon [7,9,10]. Even though a number of works were done on the sorption of metals and organic contaminants using modified activated carbon, there are few researches on the adsorption of heavy metals by manganese oxide loaded activated carbon because Mn_3O_4 is regarded as a new adsorbent [11]. Manganese oxides are a very important scavenger of aqueous trace metals in soil, sediments, and rock because of their dominant sorptive behavior [12]. Therefore, several studies have been conducted using manganese oxide-coated adsorbents to enhance adsorption capacity from aqueous solutions by using their high affinity for heavy metals [13-16]. In previous heavy metal removal studies, chemical precipitation methods were used to coat manganese oxide onto an adsorbent support, and the major form of manganese oxide was manganese dioxide (MnO_2). However, various active states of manganese and particle dispersion can be obtained using different precursors and preparation methods, which influence activity of the catalysts. Calcination temperature determines the final oxidation state of the supported manganese [17,18]. Wang et al. [19] found that Mn_3O_4-coated AC removes H_2S better than Mn_2SiO_4-coated AC due to its better dispersion on an AC support.

Supercritical techniques have been applied to produce nanoparticles and nanostructured materials as well as a generalized crystallization method to produce metal oxide particles [20-23]. The use of supercritical conditions appears to be a promising method for preparing adsorbents and can produce uniformly sized and chemically stabilized particles by optimizing reaction temperature and pressure [19].

In this study, the kinetic and isotherm characteristics of Pb(II) and Cu(II) adsorption from an aqueous solution using manganese oxide-coated activated carbon (Mn_3O_4/AC) were

conducted. A supercritical technique was used to prepare Mn_3O_4/AC to more uniformly coat the manganese oxide onto the AC. Experiments were conducted to compare the adsorption properties of Mn_3O_4/AC with those of primitive AC.

2. Materials and methods

2.1. Preparation of adsorbents

Supercritical technique was employed to synthesize metal nanoparticles, which offers great synthetic flexibility because of the unique physichochemical properties controlled by temperature and pressure [24]. Commercially available AC (Norit GAC 1240) was used to prepare the Mn_3O_4/AC in the supercritical condition. The AC was powdered to increase surface area before the manganese oxide coating. Coating of manganese oxide onto the AC was performed at high temperature (280^{o}C) and pressure (13 MPa) to create a supercritical condition. One g of AC, 3.2 g of manganese (III) acetylacetonate (Sigma-Aldrich, St. Louis, MO, USA) and 46 mL of methyl alcohol were mixed in a bomb (Parr 4748; Parr Instrument Co., Moline, IL, USA) and kept at a controlled temperature in a furnace for 2 hours. The prepared Mn_3O_4/AC was washed with ethanol and distilled water, centrifuged, and stored in a bottle.

2.2. Characterization of adsorbents

The mineralogy of the AC and Mn_3O_4/AC was characterized by X-ray diffraction (XRD) using a X-ray diffraction machine (D8 Advance, Bruker Corp., Ettlingen, Germany). The morphology and elementary composition of the adsorbent surfaces were observed using a scanning electron microscopy with energy dispersive X-ray spectrometer (SEM-EDS, JSM-

2701F, JEOL, Tokyo, Japan). Pore structure was determined via nitrogen adsorption at 77 K using a Micromeritics ASAP2010 analyzer installed in KBIS (Jeonju, Korea). Surface area and pore volume were calculated using the Brunauer–Emmett–Teller model and Barrett–Joyner–Halenda method.

2.3. Metal adsorption experiments

The adsorption characteristics of Pb(II) and Cu(II) onto the prepared Mn_3O_4/AC were investigated in a batch experiment with AC used as the control adsorbent. All chemicals and reagents used were of analytical grade. A stock solution of heavy metals was prepared by dissolving $Pb(NO_3)_2$ and $Cu(NO_3)_2$ in distilled water to a concentration of 1000 mg/L. Working solutions were prepared by diluting the stock solution to specific concentrations. For the batch test, 200 mL of the Pb(II) and Cu(II) soltuions was mixed with 0.2 g of AC, Mn_3O_4 or Mn_3O_4/AC and shaken in a shaking incubator for 48 hours.

All experiments were conducted at 30^{o}C. The initial pH was adjusted to 5.0 using 0.1 M HNO_3 or 0.1 M NaOH. Two mL samples were passed through a 0.2 μm filter (ADVANTEC, Tokyo, Japan) at predetermined time intervals (5, 10, 20, 30, 60, 120, 300, 1440, and 2880 min) then diluted with 1% nitric acid solution for the kinetic experiment. The initial concentrations were varied from 10 to 400 mg/L to reveal the isotherm properties, while other experimental condition was same with kinetic study. The concentrations of Pb(II) or Cu(II) in the solution were analyzed using inductively coupled plasma optical emission spectroscopy (5300DV, Perkin Elmer, Waltham, MA, USA). All experiments were performed in duplicate, and the average values were used.

3. Results and discussion

3.1 Physicochemical characteristics of the adsorbents

Figure 1 shows the XRD data of the AC and Mn_3O_4/AC and that of pure Mn_3O_4 powder for comparison. The figure shows that AC had no distinct peak and that manganese oxide coated onto AC had almost same peaks as pure Mn_3O_4 powder, which indicates that Mn_3O_4 is deposited on the surface of AC. Figure 2 shows the SEM images at 10,000× magnification to visualize the surface morphology of pristine AC and Mn_3O_4/AC. Rough surface shown on Mn_3O_4/AC is because of added Mn_3O_4 occupying the AC particle, whereas AC has a relatively smooth surface. It should be noted that the manganese oxide was more uniformly distributed than that of previous studies in which the manganese oxide was coated using chemical precipitation methods and formed clusters [3,16]. Therefore, the supercritical condition used in this study was expected to bring better metal ion adsorption performance.

Fig. 1. Comparison of X-ray diffraction (XRD) patterns for activated carbon (AC) and manganese oxide-coated activated carbon (Mn_3O_4/AC).

Fig. 2. Scanning electron microscopic (SEM) images of activated carbon (AC) (A) and manganese oxide-coated activated carbon (Mn_3O_4/AC) (B).

The elementary composition of the AC surface obtained from the SEM-EDS analysis was mainly carbon (94–96%) and oxygen (4–6%). A significant increase in oxygen content (31–32%) and impregnation of manganese (4–5%) was observed by coating the manganese oxide onto the AC (data not shown). The porosity and surface area of the adsorbents are

shown in Table 1. Surface area and pore volume decreased by about 50% (from 1069.3 m^2/g and 0.58 cm^3/g to 457.6 m^2/g and 0.30 cm^3/g), probably due to blocking of the AC micropores by manganese oxide, whereas pore size increased slightly from 0.41 nm to 0.57 nm after the manganese oxide coating.

3.2 Effect of the manganese oxide coating on Pb(II) and Cu(II) adsorption capacity

Figure 3 shows the comparative results of Pb(II) and Cu(II) adsorption onto Mn_3O_4/AC, and AC according to the adsorption time when the initial concentrations of metal ions were 50 mg/L at pH 5. The amounts of adsorbed Pb(II) and Cu(II) increased with time and approached equilibrium. The adsorption Pb(II) and Cu(II) progressed through two phases; an initial rapid phase where adsorption was fast and a slower second phase as observed in most heavy metal adsorption studies. The equilibrium capacities of Pb(II) and Cu(II) were 14.91 mg/g and 5.30 mg/g for AC and 49.82 mg/g and 25.66 mg/g for Mn_3O_4/AC, respectively. These results indicate that the manganese oxide coating significantly increased Pb(II) and Cu(II) adsorption capacities. It should be noted that Mn_3O_4/AC showed better adsorption capacities for Pb(II) and Cu(II) than AC, even though it's surface area was smaller than that of AC. The fact indicated that the physical adsorption onto adsorbent surface was not the only adsorption mechanism involved. The enhancement of Mn_3O_4/AC adsorption capacity might be attributed to a high negative surface charge on the modified surface. Manganese oxides are one kind of surface acidic oxides and their surface charge is negative [12,13,25].

Fig. 3. Effect of manganese oxide coating on Pb(II) and Cu(II) adsorption (adsorbent dose = 1 g/L, pH = 5, T = 30°C).

3.3 Adsorption kinetics

Pseudo-first-order and pseudo-second-order kinetic models of adsorption were used in this study. Linear regressions are frequently used to determine the best-fitting kinetic models and the least squares method is used to estimate kinetic model parameters. The linearized forms of the pseudo-first-order and pseudo-second-order models are expressed by Eq. 1 and Eq. 2.

$$\log(q_e - q_t) = \log q_e - \frac{k_1}{2.303} t \quad (1)$$

$$\frac{t}{q_t} = \frac{1}{k_2 q_e^2} + \frac{t}{q_e} \quad (2)$$

where q_e and q_t are the amount of heavy metal adsorbed per unit weight of adsorbent at equilibrium and at time t, respectively and k_1 and k_2 are the rate constants of pseudo-first-order (1/min) and second-order adsorption (g/mg min).

Figure 4 shows plots of the pseudo-first-order and second-order models for adsorbing Pb(II) and Cu(II) onto AC and Mn_3O_4/AC. The pseudo-second-order model better described the kinetics of Pb(II) and Cu(II) adsorption than the pseudo-first-order model.

Fig. 4. Pseudo-first order (A) and pseudo-second (B) order kinetics of Pb(II) and Cu(II) adsorption onto activated carbon (AC) and manganese oxide-coated activated carbon (Mn_3O_4/AC).

The kinetic constants and correlation coefficients of the pseudo-first-order and second-order models are presented in Table 2. The determination coefficients (R^2) of the pseudo-second-order kinetics were > 0.99 for adsorption of Pb(II) and Cu(II) onto both AC and Mn_3O_4/AC. Furthermore, the theoretical equilibrium capacities of Pb(II) and Cu(II) calculated by the pseudo-second-order kinetic model were almost equal to the experimentally determined adsorption capacities. The value of the pseudo-second-order rate constant (k_2) was lowest for Pb(II) adsorption onto Mn_3O_4/AC, followed by Cu(II) adsorption onto Mn_3O_4/AC, Pb(II) adsorption onto AC, and Cu(II) adsorption onto AC. This result indicated that the Mn_3O_4/AC induced faster metal adsorption onto tested adsorbents than that of AC, and that Pb(II) adsorbed faster than that of Cu(II) (The larger the k_2 value, the slower the adsorption rate). The equilibrium capacities of Mn_3O_4/AC were about 3.4 and 5.0 times higher for Pb(II) and Cu(II) than that of AC, respectively. These results indicate that coating manganese oxide onto AC significantly enhanced the adsorption capacities and kinetics. The finding that the adsorption kinetics followed pseudo-second-order model indicated that the rate limiting step of Pb(II) and Cu(II) adsorption onto AC and Mn_3O_4/AC is chemical adsorption [26,27].

The possibility of intraparticle diffusion was examined to describe the adsorption mechanism using the Weber–Morris intraparticle diffusion model expressed by Eq. 3, because the pseudo-first-order and second-order kinetic models could not describe adsorption mechanism in detail.

$$q_t \; ! \; K_d \, t^{\frac{1}{2}} \qquad (3)$$

where K_d is the intraparticle diffusion constant (mg/g $min^{1/2}$). The intraparticle diffusion plots may show multilinearity indicating that two or more steps take place [28,29]. The first, sharper portion is the external surface adsorption or instantaneous adsorption stage. The second portion is the gradual adsorption stage, where intraparticle diffusion controls the adsorption rate. The third portion is the final equilibrium stage where intraparticle diffusion starts to slow due to extremely low adsorbate concentrations in the solute [16,30,31].

Figure 5 shows the intraparticle diffusion plots for Pb(II) and Cu(II) adsorption onto Mn_3O_4/AC and AC, indicating that adsorption of metal ions onto the adsorbents occurred in three phases. Table 3 shows the intraparticle diffusion coefficients calculated from the slope of the second linear stage (Fig. 5). The determination coefficients (R^2) were > 0.94, indicating that the intraparticle diffusion model adequately described the adsorption mechanism. The intercept C value provides information related to the thickness of the boundary layer [32]. Larger intercepts suggest that surface diffusion has a larger role as the rate-limiting step [30]. The C values increased from 8.66 to 39.12 for Pb(II) and from 4.23

199 to 10.67 by coating of manganese oxide onto AC, indicating that the surface diffusion
200 became more important. The increase in the intercept C might be attributed to a reduced
201 role of intraparticle diffusion as a rate-limiting step. The results of the kinetic studies
202 indicate that the adsorption mechanisms might be a chemical adsorption process with a
203 significant contribution by intraparticle diffusion and that the resistance of intraparticle
204 diffusion decreased following the manganese oxide coating.

205 Fig. 5. Intraparticle diffusion plots for Pb(II) and Cu(II) adsorption onto manganese oxide-
206 coated activated carbon (Mn_3O_4/AC) and activated carbon (AC).

207 3.3 Adsorption isotherms

208 Langmuir and Freundlich models were used to investigate the isotherm of Pb(II) or Cu(II)
209 adsorption onto AC and Mn_3O_4/AC. The Langmuir model, which is valid for monolayer
210 adsorption onto an adsorbent surface containing a finite number of identical sites, is
211 expressed as the following linearized form (Eq. 4):

$$\frac{C_e}{q_e} = \frac{1}{Q^O b} + \frac{C_e}{Q^0} \qquad (4)$$

212 where C_e is the equilibrium concentration of the solution (mg/L), Q^0 is the monolayer
213 adsorption capacity (mg/g) and b is a constant (L/mg) related to the free energy or net
214 enthalpy of adsorption [27,33].

The linearized form of the Freundlich equation, which was derived to model the multilayer adsorption and for the adsorption on heterogeneous surfaces, is expressed by Eq. 5.

$$\log q_e \; ! \; \log K_f \; ! \; \frac{1}{n} \log C_e \qquad (5)$$

where K_f is the relative sorption capacity constant of the adsorbent ((mg/g)(L/mg)$^{1/n}$) and 1/n is the intensity of the sorption constant [27,33]. The linearized forms of the Langmuir and Freundlich adsorption isotherms and the corresponding constants are shown in Fig. 6 and Table 4. The Langmuir model gave a better fit to the experimental data over the experimental range with good determination coefficients than that of the Freundlich model, whereas the Freundlich isotherm model also described Pb(II) adsorption onto Mn_3O_4/AC well (R^2, 0.99) (Table 4). The maximum adsorption capacities of Pb(II) and Cu(II), as indicated by the Langmuir constant, Q^0, were 27.17 mg/g and 6.09 mg/g for AC and 59.52 mg/g and 37.04 mg/g for Mn_3O_4/AC, indicating 2.2 and 6.1 times enhancement for Pb(II) and Cu(II) by the manganese oxide coating onto AC. Maximum adsorption capacity of Mn_3O_4 (7.57 mg/g for Pb and 1.24 mg/g for Cu) was very low compared to that of Mn_3O_4/AC, which might be attributed to large particle size of pure commercial Mn_3O_4. Particle size of commercial Mn_3O_4 is less than 43 μm while particle size of doped Mn_3O_4 on AC under supercritical condition is less than 10 nm. Manganese acetylacetonate dissolved in methyl alcohol under supercritical condition is impregnated by activated carbon, which results in the growth of Mn_3O_4 nanoparticles on surface of activated carbon under the anchoring of –COOH and –OH groups. As it is shown from SEM image plenty of nanoparticles are well dispersed forming a coating layer on the surface of activated carbon, thereby leading to enhanced metal adsorption on the surface of Mn_3O_4/AC.

Lead and Cu can be adsorbed by Mn_3O_4/AC both through electrostatic interaction and surface complexation. Enhanced metal adsorption by Mn_3O_4/AC composite is the result of synergetic effect at the heterojunction interfaces formed between Mn_3O_4 and activated carbon as well as increased Mn_3O_4 surface area. In addition, Mn_3O_4 loaded on AC reduced resistance of intraparticle diffusion.

The Freundlich constant, n of Pb(II) adsorption at equilibrium, was > 1, indicating that metal ions were favorably adsorbed by the AC and Mn_3O_4/AC [34]. The increase in the n value of Mn_3O_4/AC for Pb(II) adsorption shows that favorability was enhanced by the manganese oxide coating onto the AC.

Fig. 6. Langmuir (A) and Freundlich (B) absorption isotherms of Pb(II) and Cu(II) by activated carbon (AC) and manganese oxide-coated activated carbon (Mn_3O_4/AC).

Maximum adsorption capacities of Pb(II) and Cu(II) obtained in this study are compared with those of other studies in Table 5. The significant enhancement of metal ion adsorption onto Mn_3O_4/AC observed in this study was comparable to the results of previous studies that used various adsorbents such as carbon nanotubes, zeolite, and sand, indicating that manganese oxide is an effective coating material to enhance the adsorption capacities of Pb(II) and Cu(II). In particular, Mn_3O_4/AC showed an outstanding adsorption capacity for Cu(II) while it had a similar adsorption capacity for Pb(II) compared to MnO_2/Zeolite [12]. The results of the isotherm study show that Mn_3O_4/AC is a competent adsorbent to remove metal ions from aqueous solutions.

4. Conclusions

The uniformly distributed Mn_3O_4-coated AC was obtained by using the supercritical technique and it's adsorption properties for Pb(II) and Cu(II) were compared with those of AC. The manganese oxide coating significantly enhanced the adsorption capacities of Pb(II) and Cu(II). The pseudo-second-order kinetic model better described Pb(II) and Cu(II) adsorption by AC and AC/Mn_3O_4 than that of the pseudo-first-order model, indicating that the rate limiting step of the adsorption was chemical adsorption. The adsorption mechanism was controlled by intraparticle diffusion, and the resistance of intraparticle diffusion decreased by the manganese oxide coating. The Langmuir isotherm model provided a better fit to the experimental data than did the Freundlich isotherm model. The maximum adsorption capacities of Pb(II) and Cu(II) obtained by Langmuir constant were 27.17 mg/g and 6.09 mg/g for AC and 59.52 mg/g and 37.04 mg/g for Mn_3O_4/AC, indicating 2.2 and 6.1 times enhancement for Pb(II) and Cu(II) by the manganese oxide coating onto AC. These results indicate that Mn_3O_4/AC is a competent adsorbent to remove heavy metals from aqueous solutions.

Acknowledgements

This study was supported by the Korea Ministry of Environment as "The GAIA Project" (G112-17003-0043-0).

References

[1] X. Zhao, G. Zhang, Q. Jia, C. Zhao, W. Zhou, W. Li, Chemical Engineering Journal 171 (2011) 152.

[2] D. Mohan, K.P. Singh, Water Research 36 (2002) 2304.

278 [3] R. Han, Z. Lu, W. Zou, W. Daotong, J. Shi, Y. Jiujun, Journal of Hazardous Materials
279 B137 (2006) 480.
280 [4] D. Mohan, C.U. Pittman, Journal of Hazardous Materials B137 (2006) 762.
281 [5] L. Li, P.A. Quinlivan, D.R.U. Knappe, Carbon 40 (2002) 2085.
282 [6] D. Mugisidi, A. Ranaldo, J.W. Soearsono, M. Hikam, Carbon 45 (2007) 1081.
283 [7] S. Khodadoust, M. Ghaedi, R. Sahraei, A. Daneshfar, Journal of Industrial and
284 Engineering Chemistry (2013), http://dx.doi.org/10.1016/j.jiec.2013.10.053.
285 [8] J. Rivera-Utrilla, M. Sánchez-Polo, V. Gómez-Serrano, P.M. Álvarez, M.C.M. Alvim-
286 Ferraz, J.M. Dias, Journal of Hazardous Materials 187 (2011) 1-23.
287 [9] M. Ghaedi, A. Ansari, M.H. Habibi, A.R. Asghari, Journal of Industrial and
288 Engineering Chemistry 20 (2014) 17.
289 [10] S. Khodadoust, M. Ghaedi, R. Sahraei, A. Daneshfar, Journal of Industrial and
290 Engineering Chemistry 19 (2013), 1209.
291 [11] G. An, P. Yu, M. Xiao, Z. Liu, Z. Miao, K. Ding, L. Mao, Nanotechnology 19 (2008)
292 1.
293 [12] W. Zou, R. Han, Z. Chen, Z. Jinghua, J. Shi, Physicochemical and Engineering
294 Aspects, 279 (2006) 238.
295 [13] E. Allen, G. Fu, C. Cowan, Soil Science 152 (1991) 72.
296 [14] D. Tiwari, C. Laldanwngliana, C.H. Choi, S.M. Lee, Chemical Engineering Journal
297 171 (2011) 958.
298 [15] S.G. Wang, W.X. Gong, X.W. Liu, Y.W. Yao, B.Y. Gao, Separation and Purification
299 Technology 58 (2007) 17.

[16] W. Zou, R. Han, Z. Chen, J. Shi, L. Hongmin, Journal of Chemical & Engineering Data 51 (2006) 534.

[17] W.J.W. Bakker, F. Kapteijn, J.A. Moulijn, Chemical Engineering Journal 96 (2003) 223.

[18] Y. Ma, S.G. Wang, M.H. Fan, W.X. Gong, B.Y. Gao, Journal of Hazardous Materials 168 (2009) 1140.

[19] J. Wang, B. Qiu, L. Han, G. Feng, Y. Hu, L. Chang, W. Bao, Journal of Hazardous Materials 213-214 (2012) 184.

[20] A. Aimable, H. Muhr, C. Gentric, F. Bernard, F. le Cras, D. Aymes, Powder Technology 190 (2009) 99.

[21] K. Byrappa, T. Adschiri, Progress in Crystal Growth and Characterization of Materials 53 (2007) 117.

[22] P.A. Marrone, G.T. Hong, M.H. Spritzer, Journal of Advanced Oxidation Technologies 10 (2007) 157.

[23] E. Reverchon, R. Adami, Journal of Supercritical Fluids 37 (2006) 1.

[24] H. Choi, B. Veriansyah, J. Kim, J.D. Kim, J.W. Kang, The Journal of Supercritical Fluids 52 (2010)285.

[25] J. Murray, Journal of Colloid and Interface Science 46 (1974) 357.

[26] Y.S. Ho, G. McKay, Process Biochemistry 34 (1999) 451.

[27] F.M. Pellera, A. Giannis, D. Kalderis, K. Anastasiadou, R. Stegmann, J.Y. Wang, E. Gidarakos, Journal of Environmental Management 96 (2012) 35.

[28] E.I. Unuabonah, K.O. Adebowale, B.I. Olu-Owolabi, Journal of Hazardous Materials 144 (2007) 386.

323 [29] F.C. Wu, R.L. Tseng, R.S. Juang, Chemical Engineering Journal 153 (2009) 1.

324 [30] H.K. Boparai, M. Joseph, D.M. O'Carroll, Journal of Hazardous Materials 186 (2011)

325 458.

326 [31] Q.S. Liu, T. Zheng, P. Wang, J.P. Jiang, N. Li, Chemical Engineering Journal 157

327 (2010) 348.

328 [32] D. Kavitha, C. Namasivayam, Bioresource Technology 98 (2007) 14.

329 [33] Z. Liu, F.S. Zhang, Journal of Hazardous Materials 167 (2009) 933.

330 [34] Z. Aksu, Process Biochemistry 38 (2002) 89.

331 [35] J. Goel, K. Kadirvelu, C, Rajagopal, V.K. Garg, Journal of Hazardous Materials B125

332 (2005) 211.

333 [36] Y.H. Li, S.G. Wang, J.Q. Wei, X.F. Zhang, C.L. Xu, Z.K. Luan, D.H. Wu, B.Q. Wei,

334 Chemical Physics Letters 357 (2002) 263.

335 [37] M. Imamoglu, Q. Tekir, Desalination 228 (2008) 108.

336

336 **Figure Captions**

337 Fig. 1. Comparison of X-ray diffraction (XRD) patterns for activated carbon (AC) and
338 manganese oxide-coated activated carbon (Mn_3O_4/AC).

339 Fig. 2. Scanning electron microscopic (SEM) images of activated carbon (AC) (A) and
340 manganese oxide-coated activated carbon (Mn_3O_4/AC) (B).

341 Fig. 3. Effect of manganese oxide coating on Pb(II) and Cu(II) adsorption (adsorbent dose
342 = 1 g/L, pH = 5, T = 30^{o}C).

343 Fig. 4. Pseudo-first order (A) and pseudo-second (B) order kinetics of Pb(II) and Cu(II)
344 adsorption onto activated carbon (AC) and manganese oxide-coated activated carbon
345 (Mn_3O_4/AC).

346 Fig. 5. Intraparticle diffusion plots for Pb(II) and Cu(II) adsorption onto manganese oxide-
347 coated activated carbon (Mn_3O_4/AC) and activated carbon (AC).

348 Fig. 6. Langmuir (A) and Freundlich (B) absorption isotherms of Pb(II) and Cu(II) by
349 activated carbon (AC), manganese oxide (Mn_3O_4) and manganese oxide-coated activated
350 carbon (Mn_3O_4/AC).

Table 1. Porosity and surface area properties of the adsorbents

Sample	Pore size (nm)	BET surface area (m^2/g)	Pore volume (cm^3/g)
AC	0.41	1069.3	0.58
Mn_3O_4/AC	0.57	457.6	0.30

Table 2. First-order and second-order kinetic parameters for Pb(II) and Cu(II) adsorption on activated carbon (AC) and manganese oxide-coated activated carbon (Mn_3O_4/AC) at 303 K

Metal	Adsorbent	q_e(exp.) (mg/g)	First-order rate constants			Second-order rate constants		
			k_1 (min^{-1})	q_e(theor.) (mgg^{-1})	R^2	k_2 (g/mg min)	q_e(theor.) (mg/g)	R^2
Pb	AC	14.91	0.0012	8.44	0.749	0.0013	14.82	0.996
	Mn_3O_4/AC	49.82	0.0021	21.95	0.774	0.0008	50.00	0.999
Cu	AC	5.30	0.0032	2.24	0.874	0.0103	5.13	1.000
	Mn_3O_4/AC	25.66	0.0012	17.62	0.901	0.0005	25.71	0.994

Table 3. Intraparticle diffusion coefficients and intercept values for Pb(II) and Cu(II) adsorption onto activated carbon (AC) and manganese oxide-coated activated carbon (Mn_3O_4/AC) at 303 K

Metal	Adsorbent	K_d (mg/g $min^{1/2}$)	Intercept value (C)	R^2
Pb(II)	AC	0.1178	8.66	0.964
	Mn_3O_4/AC	0.2144	39.12	0.939
Cu(II)	AC	0.0228	4.23	0.945
	Mn_3O_4/AC	0.288	10.67	0.992

Table 4. Isotherm parameters for Pb(II) and Cu(II) adsorption onto activated carbon (AC), manganese oxide (Mn_3O_4) and manganese oxide-coated activated carbon (Mn_3O_4/AC) at 303 K

Metal	Adsorbent	Langmuir isotherm			Freundlich isotherm		
		Q^0(mg/g)	b	R^2	K_f	n	R^2
Pb	AC	27.17	0.04	0.993	4.88	3.45	0.989
	Mn_3O_4	7.57	0.02	0.945	1.85	4.85	0.838
	Mn_3O_4/AC	59.52	0.31	0.999	47.42	25.64	0.991
Cu	AC	6.09	0.79	0.994	3.39	8.33	0.549
	Mn_3O_4	1.24	0.03	0.983	165.20	0.24	0.774
	Mn_3O_4/AC	37.04	0.06	0.992	15.60	7.28	0.892

367 Table 5. Equilibrium capacities of Pb(II) and Cu(II) by various adsorbents

Metal ion	Adsorbent	Q^0 (mg/g)	pH	Reference
Pb(II)	AC	21.88	5	[35]
	AC-S	29.44	5	[35]
	CNTs	17.44	5	[36]
	MnO_2/CNTs	78.74	5	[15]
	Zeolite	27.76*	5	[12]
	MnO_2/Zeolite	60.08	4	[12]
	MnO_2/Sand	1.77	4	[3]
	AC	27.17	5	This study
	Mn_3O_4/AC	59.52	5	This study
Cu(II)	AC	6.65	5.7	[37]
	MnO_2/Sand	0.41	4	[3]
	Zeolite	3.88*	5	[12]
	MnO_2/Zeolite	8.20	4	[12]
	AC	6.09	5	This study
	Mn_3O_4/AC	37.04	5	This study

368 * Maximum adsorption capacities were experimentally determined values.

Graphical Abstract (for review)

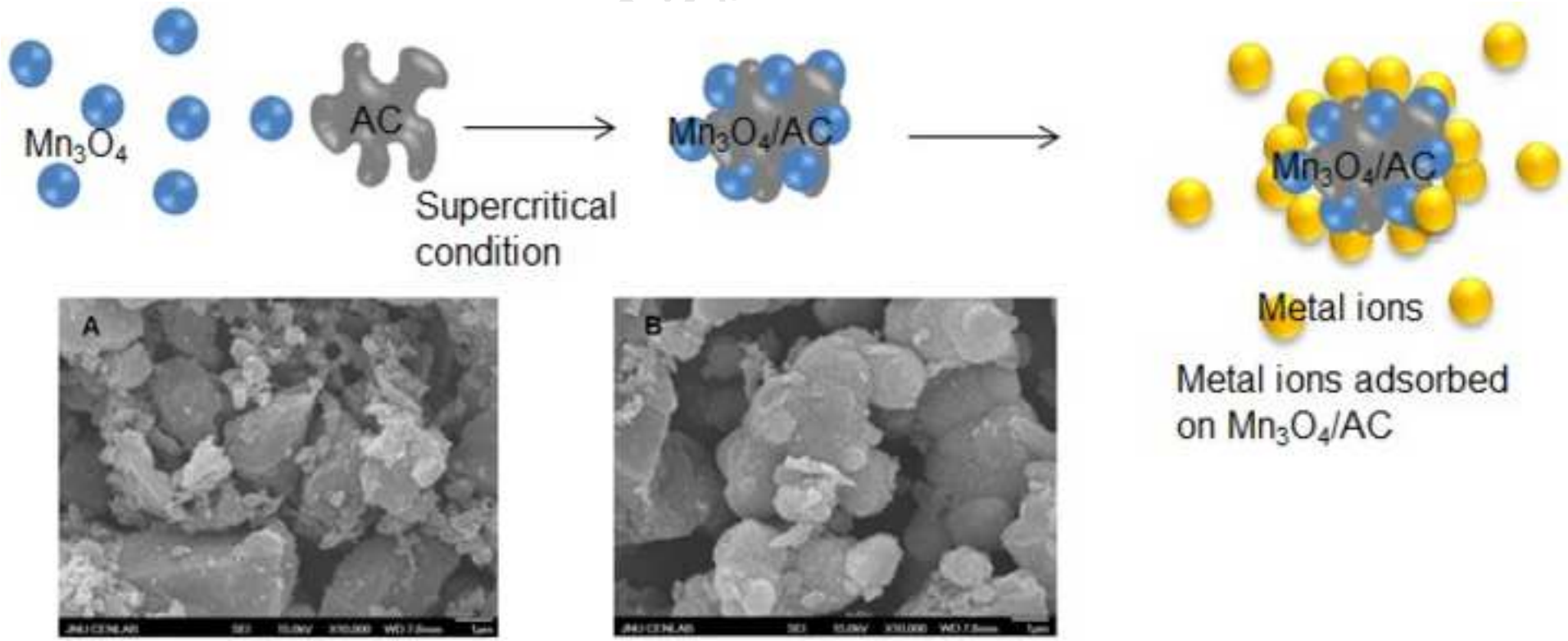

Figure 1

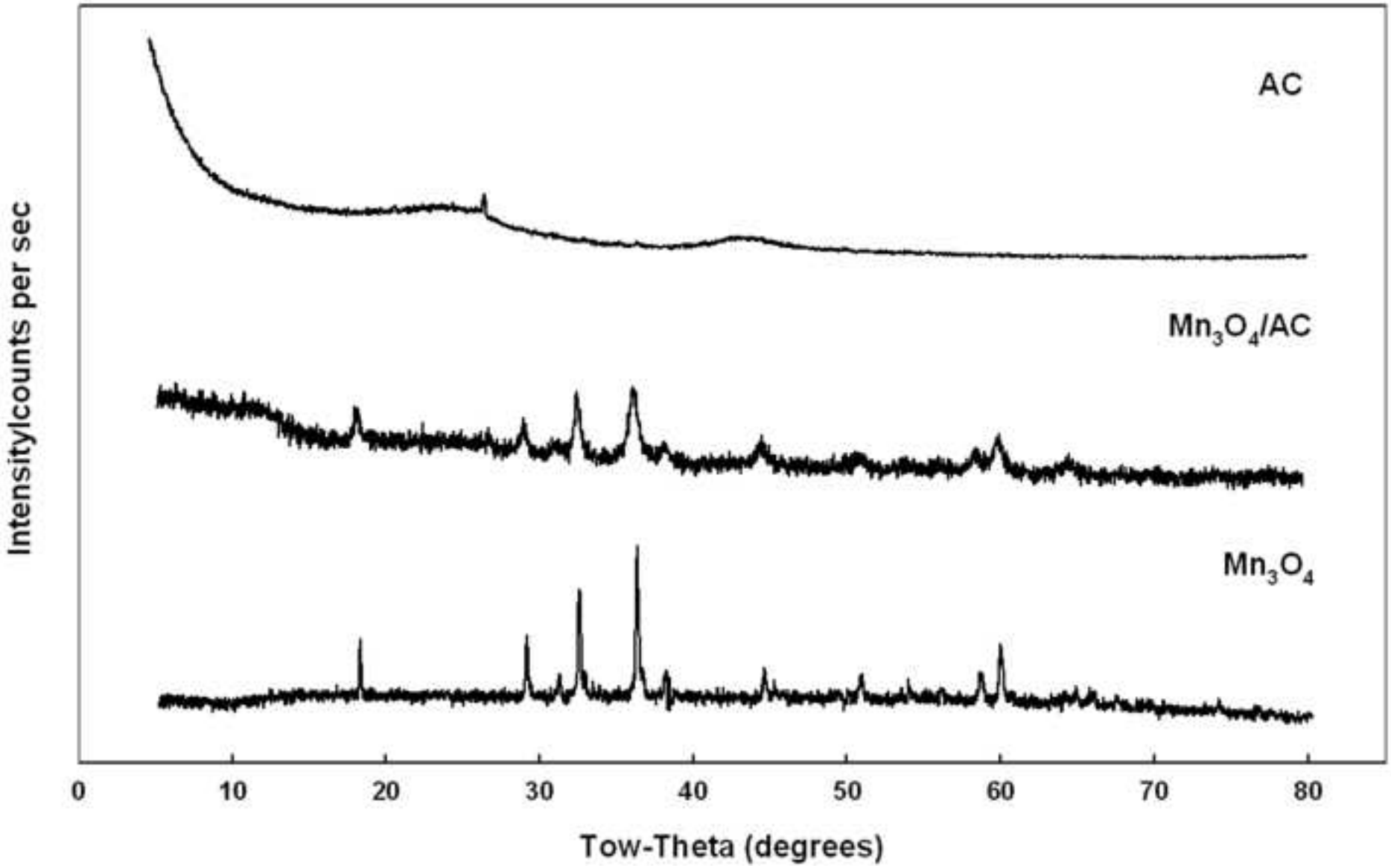
AC
Mn3O4/AC
Mn3O4
Intensitylcounts per sec
0
10
20
30
40
50
60
70
80
Tow-Theta (degrees)

Figure 2(A)

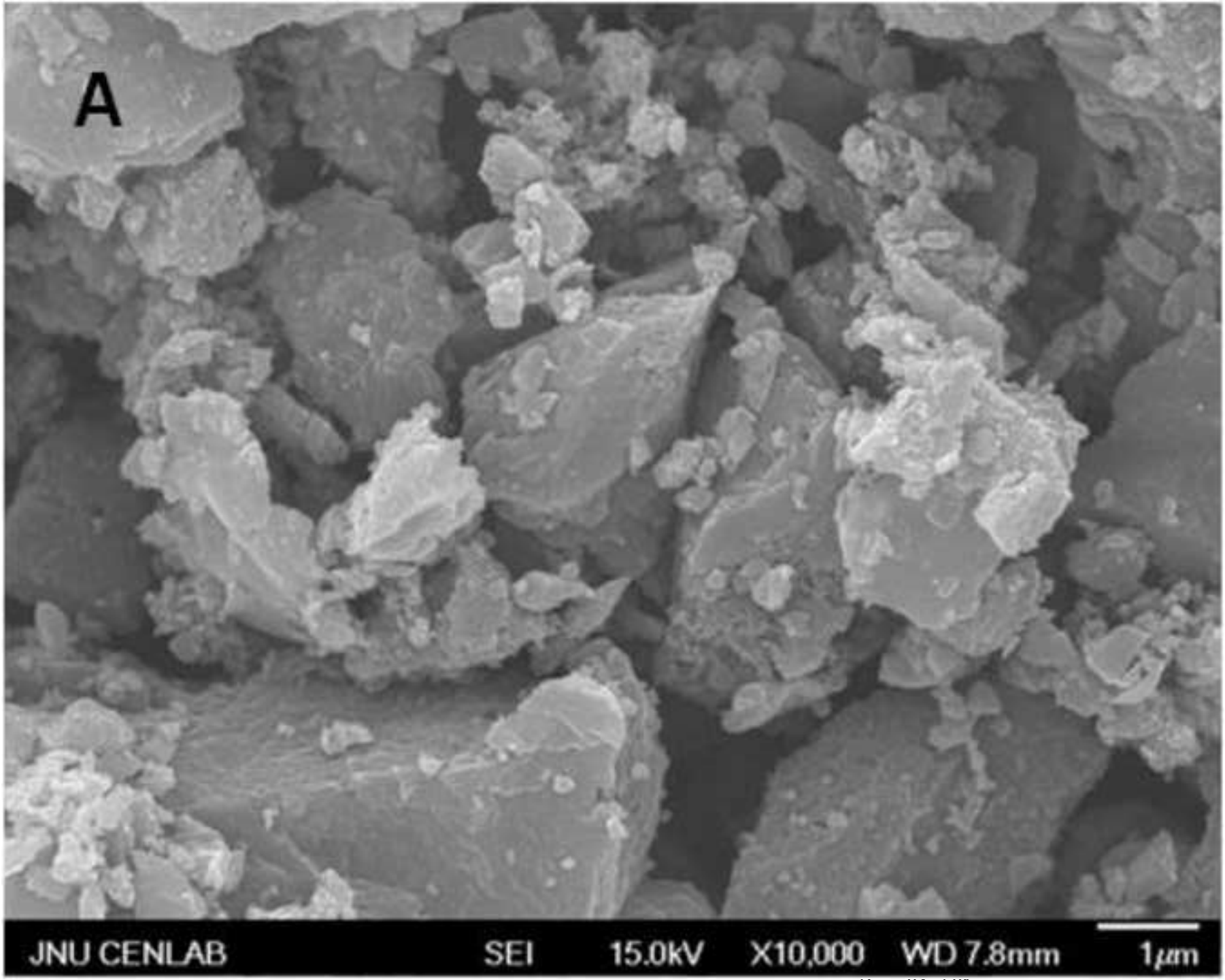

Figure 2(B)

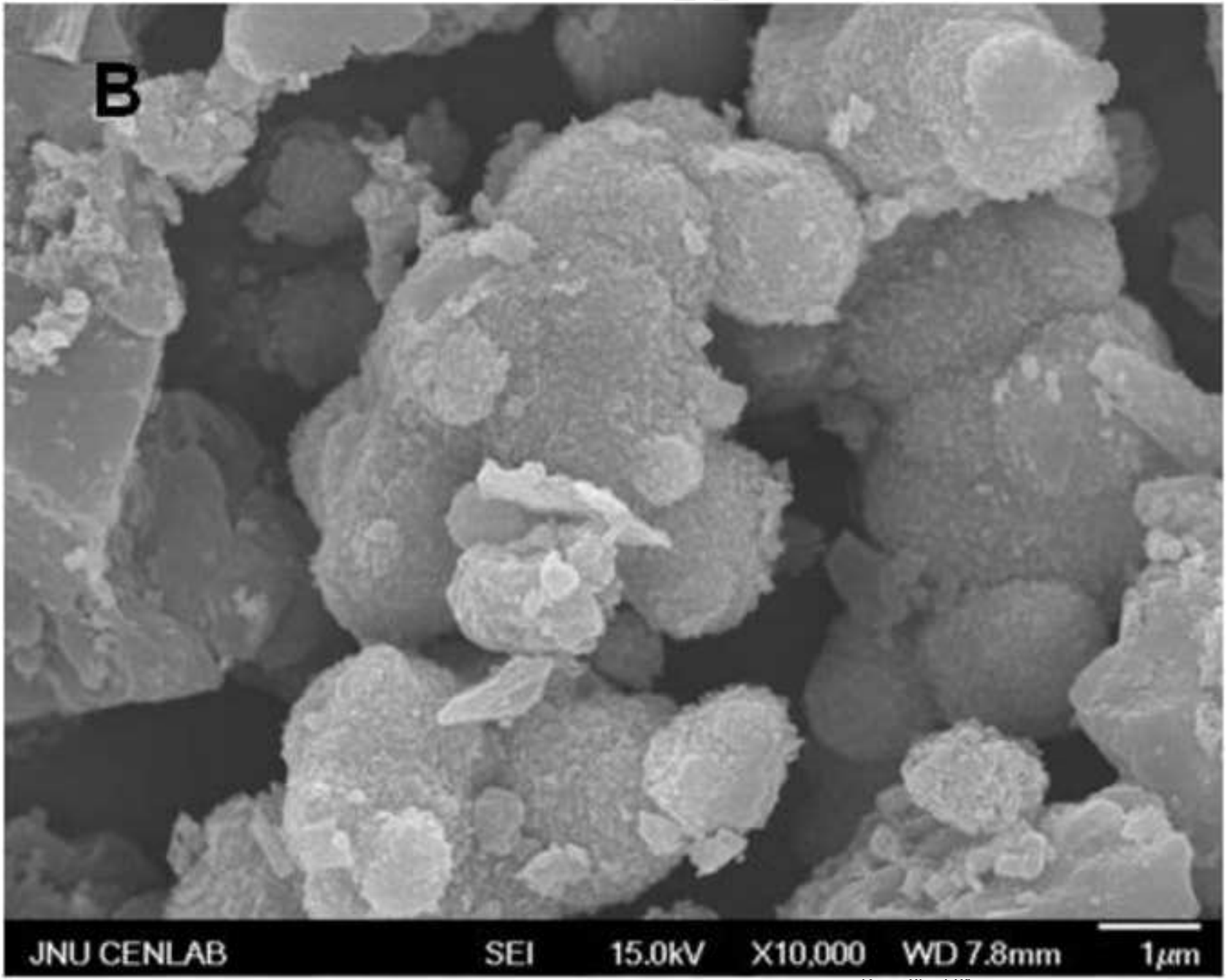

Figure 3

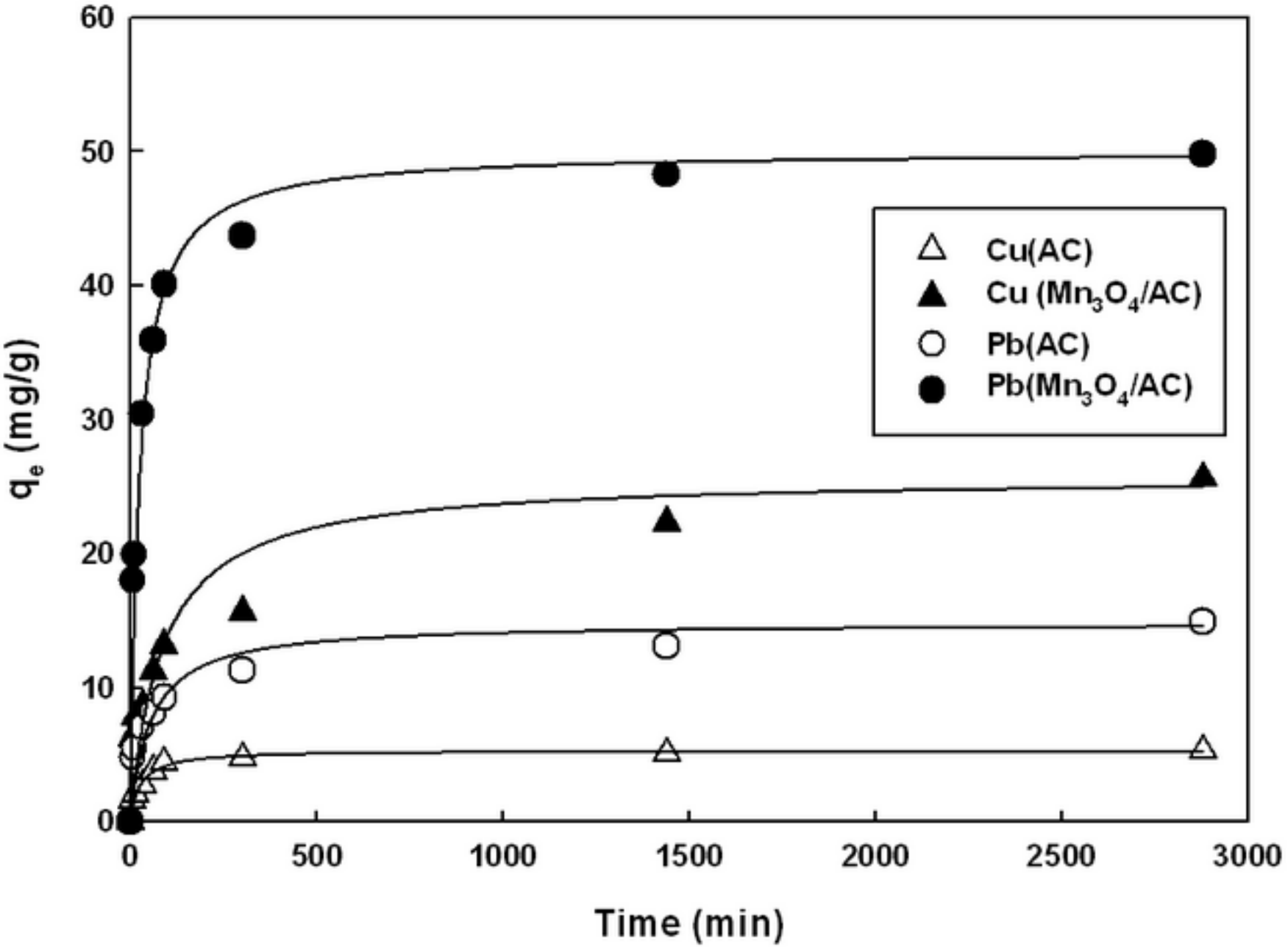
60
50
40
30
20
10
0
0
500
1000
1500
2000
2500
3000
q_e (mg/g)
Time (min)
Cu(AC)
Cu (Mn_3O_4/AC)
Pb(AC)
Pb(Mn_3O_4/AC)

Figure 4(A)

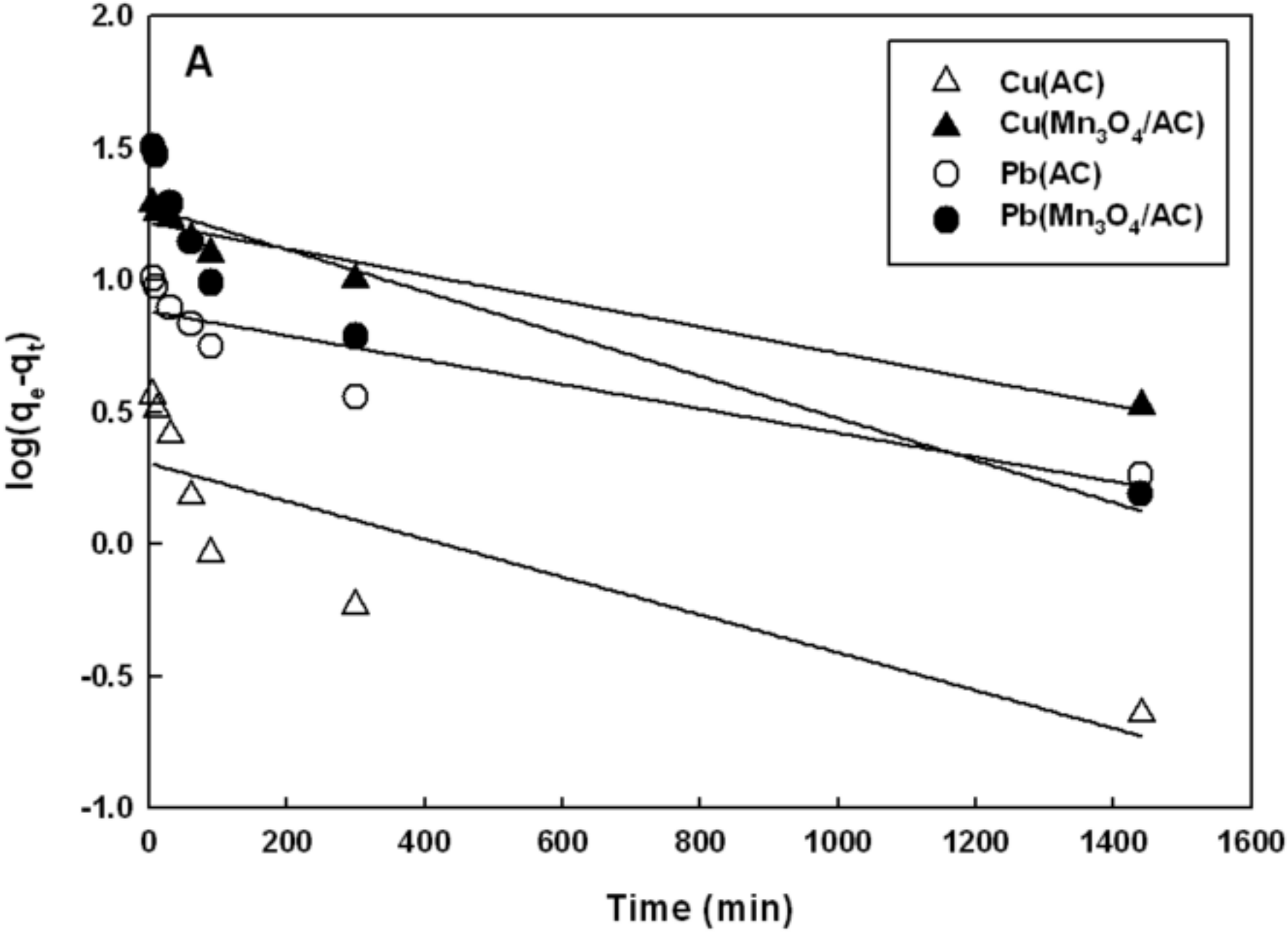
A
Cu(AC)
Cu(Mn3O4/AC)
Pb(AC)
Pb(Mn3O4/AC)
log(qe-qt)
Time (min)
2.0
1.5
1.0
0.5
0.0
-0.5
-1.0
0
200
400
600
800
1000
1200
1400
1600

Figure 4(B)

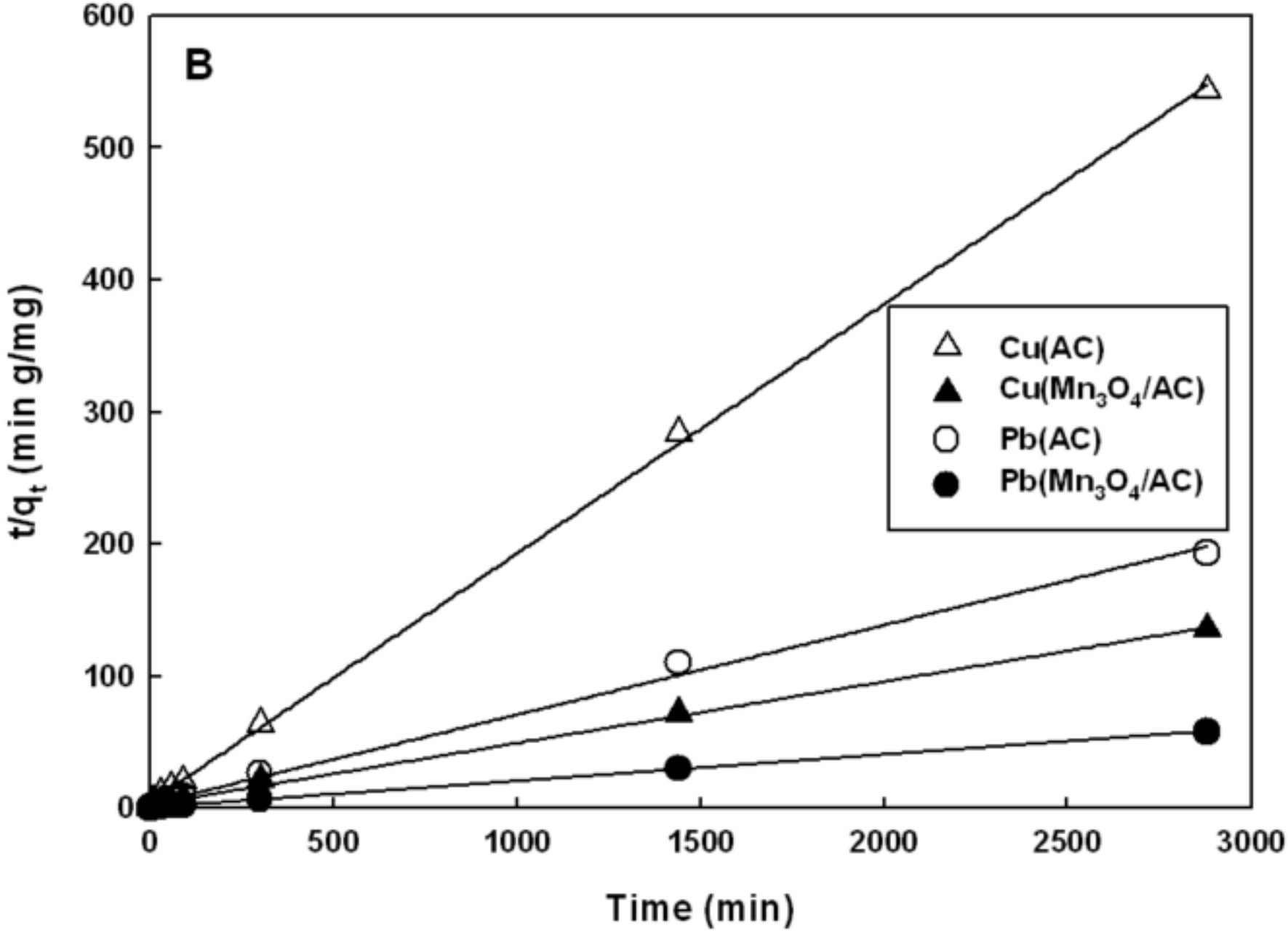
B
600
500
400
300
200
100
0
0
500
1000
1500
2000
2500
3000
t/q_t (min g/mg)
Time (min)
Cu(AC)
Cu(Mn3O4/AC)
Pb(AC)
Pb(Mn3O4/AC)

Figure 5

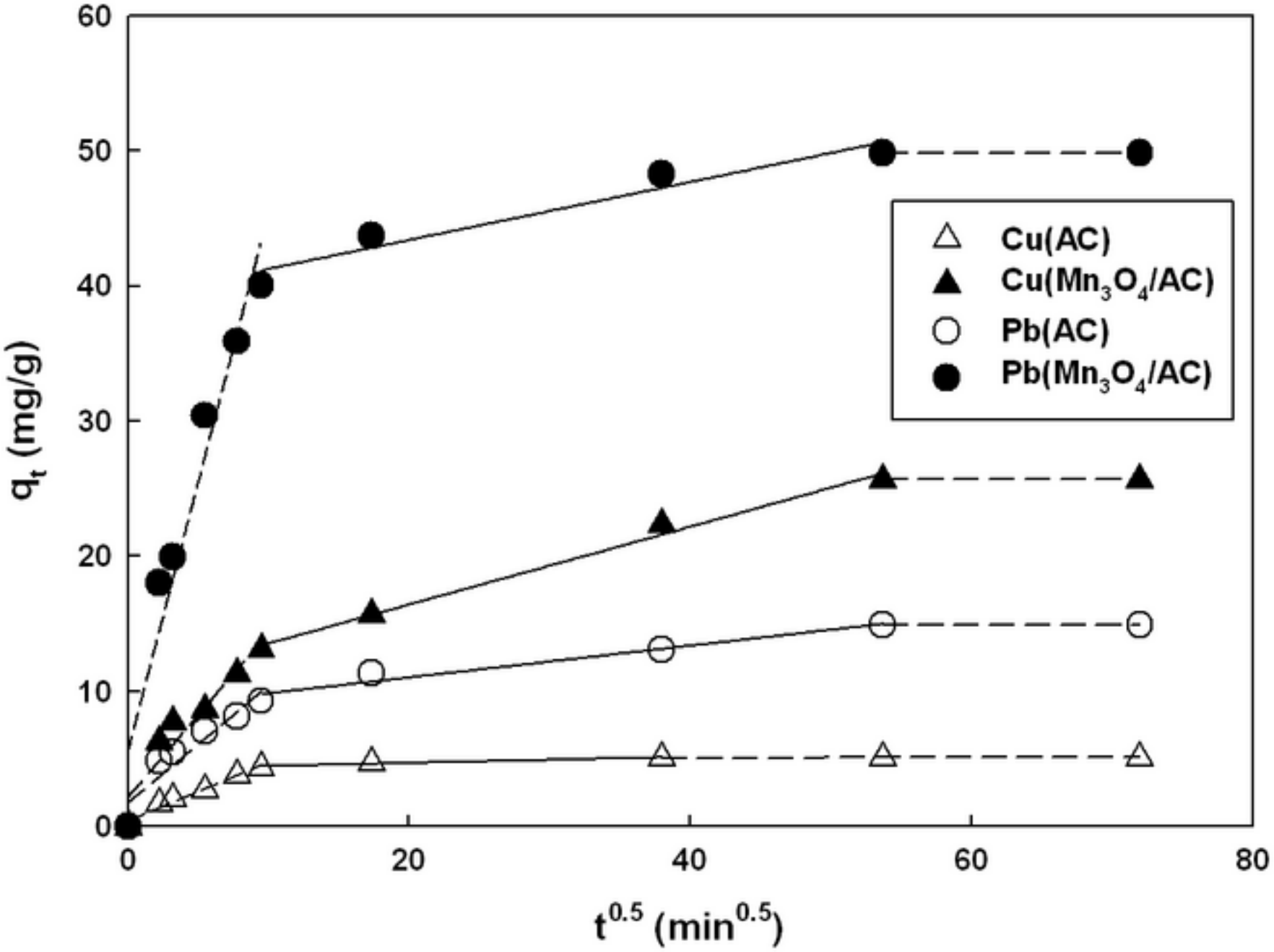
60
50
40
30
20
10
0
0
20
40
60
80
q_t (mg/g)
$t^{0.5}$ ($min^{0.5}$)
Cu(AC)
Cu(Mn_3O_4/AC)
Pb(AC)
Pb(Mn_3O_4/AC)

Figure 6(A)

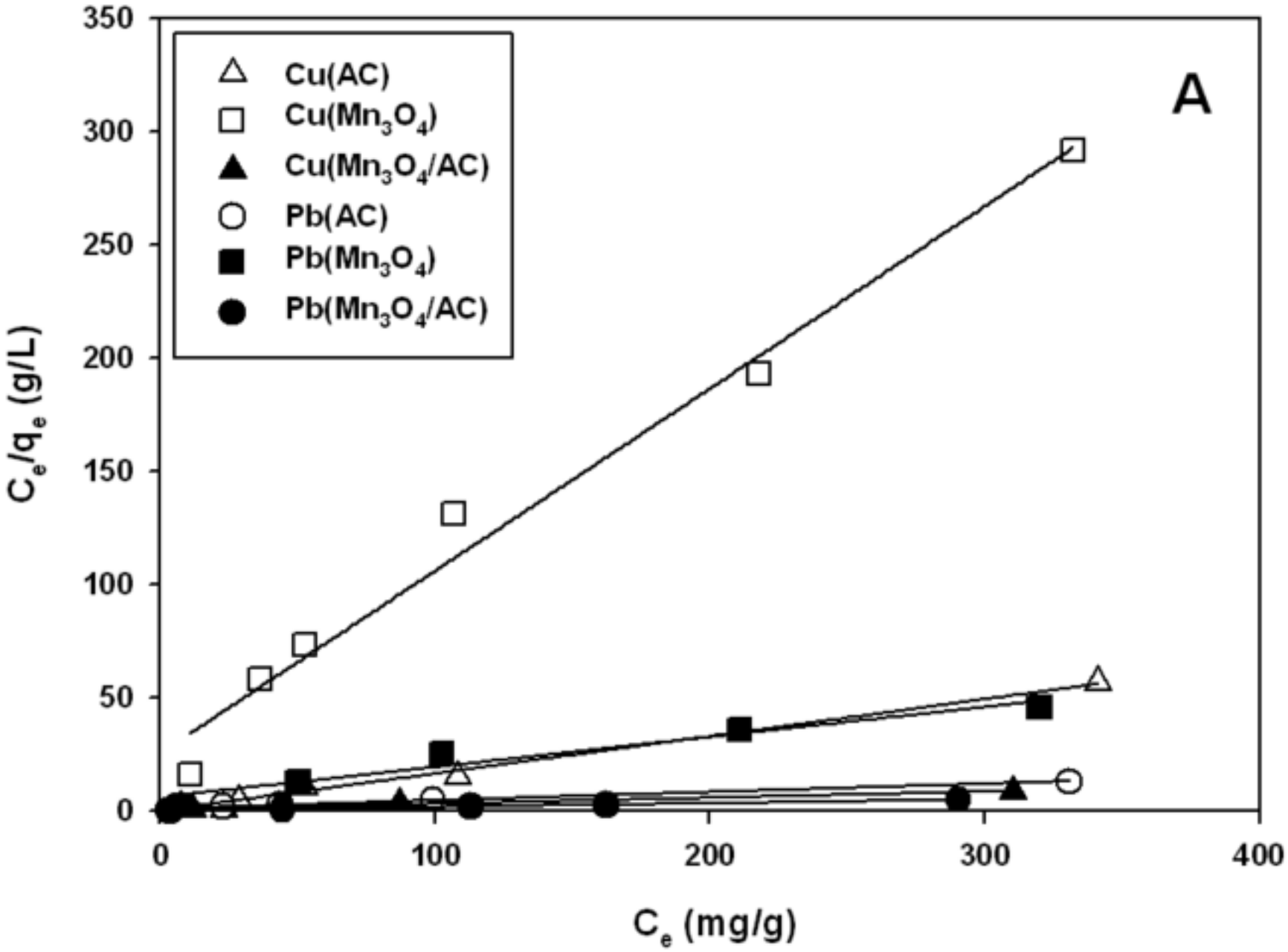
A
Cu(AC)
Cu(Mn3O4)
Cu(Mn3O4/AC)
Pb(AC)
Pb(Mn3O4)
Pb(Mn3O4/AC)
Ce/qe (g/L)
Ce (mg/g)
0
50
100
150
200
250
300
350
0
100
200
300
400

Figure 6(B)

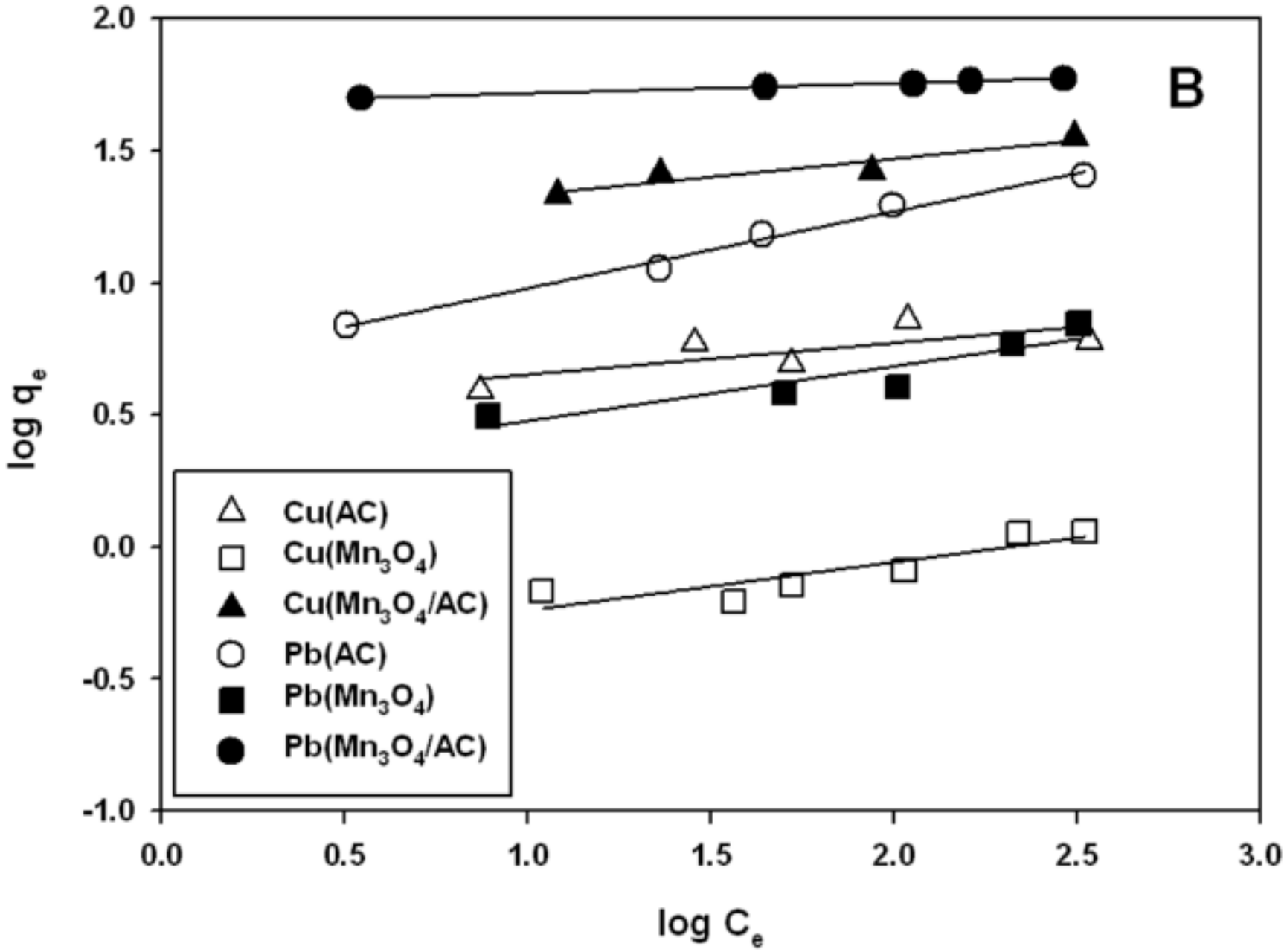
B
log q_e
log C_e
2.0
1.5
1.0
0.5
0.0
-0.5
-1.0
0.0
0.5
1.0
1.5
2.0
2.5
3.0
Cu(AC)
Cu(Mn_3O_4)
Cu(Mn_3O_4/AC)
Pb(AC)
Pb(Mn_3O_4)
Pb(Mn_3O_4/AC)